Chemical Science

ROYAL SOCIETY OF CHEMISTRY

EDGE ARTICLE

View Article Online
View Journal | View Issue

Cite this: *Chem. Sci.*, 2024, **15**, 20315

All publication charges for this article have been paid for by the Royal Society of Chemistry

Rare-earth metal complexes bearing electrophilic and nucleophilic carbon centres and their unique reactivity patterns towards pyridine derivatives†

Weikang Wu,[a] Thayalan Rajeshkumar,[d] Shan Zhu,[a] Fuxiang Chai,[a] Dongjing Hong,[a] Zeming Huang,[b] Qingbing Yuan,[a] Laurent Maron *[d] and Shaowu Wang *[bc]

The rare-earth metal dialkyl complexes (κ^2-L^1)RE(CH_2SiMe_3)$_2$·(THF)$_2$ [RE = Lu(**1a**), Yb(**1b**), Er(**1c**), Y(**1d**), Dy(**1e**)] (L^1 = 1-(2-*N*-$C_5H_{10}NCH_2CH_2$)-3-(2,6-^{i}Pr$_2$$C_6H_3$N=CH)-$C_8H_4$N) and the rare-earth metal monoalkyl complexes (κ^2-L^1)$_2$RE(CH_2SiMe_3)·(THF)$_n$ [n = 0, RE = Lu(**2a**), Yb(**2b**); n = 1, Er(**2c**), Y(**2d**), Dy(**2e**)], (κ^2-L^2)$_2$RE(CH_2SiMe_3)·THF [RE = Yb(**3a**), Er(**3b**), Y(**3c**), Dy(**3d**), Gd(**3e**)] (L^2 = 1-(2-*N*-$C_5H_{10}NCH_2CH_2$)-3-(AdN=CH)-C_8H_4N) (Ad = adamantyl, $C_{10}H_{15}$) have been synthesized and fully characterized. These complexes feature chelate ligands having a conjugated system (–C=C–C=N) with an sp^2 carbon, which enables both electrophilic and nucleophilic carbon centres to be directly connected to the highly electrophilic rare-earth metal ions. The reactions of these complexes with different pyridine derivatives have been systematically investigated with the discovery of reactivity patterns distinct from those of previously reported transition metal complexes. These unusual reactivity patterns include consecutive C–H activation/1,1-migratory insertion/C–N and C–H activation, C–H activation/1,1-migratory insertion/C–N bond activation, C–H activation/1,1-migratory insertion, and homolytic redox reactions. DFT calculation results together with experimental evidences support the key mechanistic proposal that the indol-2-yl carbon of the ligands exhibits electrophilic carbene character accounting for the subsequent 1,1-migratory insertion reaction after C–H activation.

Received 25th June 2024
Accepted 5th November 2024

DOI: 10.1039/d4sc04197f

rsc.li/chemical-science

Introduction

Pyridine and its derivatives, as an important class of pharmaceutical platform, are widely used in drug design and also play crucial roles in organic synthesis, inorganic materials and organometallic chemistry. Transformation of pyridine derivatives is thus a great interest of current synthetic chemistry.[1] Since the initial report on cyclometallation reactions of titanium alkyl complexes with pyridines in 1981,[2] a range of transition metal and rare-earth metal alkyl or hydrido complexes have been studied in such cyclometallation reactions (Scheme 1a),[3,5a,6d] and 1,2- and 1,4-benzyl additions to the pyridine ring of 2-phenylpyridine were occasionally observed (Scheme 1a).[4] After activation of the sp^2 C–H bond on the pyridine or the phenyl ring of 2-phenylpyridine, the resulting three- or five-membered metallacycles can react with hydrogen, Lewis bases, alkenes, alkynes, selenium and carbon monoxide to produce various functionalized pyridine derivatives.[5,6] However, to date, the migratory insertion of the three-membered metallacycles to the electrophilic carbon bonded to the rare-earth metal centre has not yet been reported, and the sp^3 C–H activation of 2-*N*,*N*-dimethylaminopyridine followed by 1,1-migratory insertion and C–N bond cleavage also remains elusive.

Meanwhile, the 2,2′-bipyridyl radical anion is commonly obtained by the reactions of low-valent rare-earth metal complexes with 2,2′-bipyridine (Scheme 2, method 1).[7] Alternatively, 2,2′-bipyridyl anionic radical rare-earth or actinide metal complexes can also be obtained by treatment of the corresponding complexes with 2,2′-bipyridine in the presence of KC_8 (Scheme 2, method 2).[8] Following these two methods, a range of rare-earth metal and actinide complexes containing the 2,2′-bipyridyl anionic radical have been reported,[8b,c,9–14] and they showed unique reactivity towards various organic or inorganic molecules.[8b,d–g,9–14] Notably, in the reaction of 1,3-butadiene Sc(III) complex with 2,2′-bipyridine,[15] it was proposed to involve a Sc(III) to Sc(I) reaction pattern to produce the scandium

[a]*Key Laboratory of Functional Molecular Solids, Ministry of Education, Anhui Laboratory of Molecule-Based Materials, College of Chemistry and Materials Science, Anhui Normal University, Wuhu 241000, Anhui, P. R. China*

[b]*Anhui Laboratory of Clean Catalytic Engineering, Anhui Laboratory of Functional Coordinated Complexes for Materials Chemistry and Application, College of Chemical and Environmental Engineering, Anhui Polytechnic University, Wuhu 241000, Anhui, P. R. China. E-mail: wsw@ahpu.edu.cn; swwang@mail.ahnu.edu.cn*

[c]*State Key Laboratory of Organometallic Chemistry, Shanghai Institute of Organic Chemistry, Chinese Academy of Sciences, Shanghai 200032, P. R. China*

[d]*LPCNO, CNRS & INSA, Université Paul Sabatier, 135 Avenue de Rangueil, 31077 Toulouse, France. E-mail: laurent.maron@irsamc.ups-tlse.fr*

† Electronic supplementary information (ESI) available. CCDC 2278697–2278701, 2348805–2348814 and 2348816–2348844. For ESI and crystallographic data in CIF or other electronic format see DOI: https://doi.org/10.1039/d4sc04197f

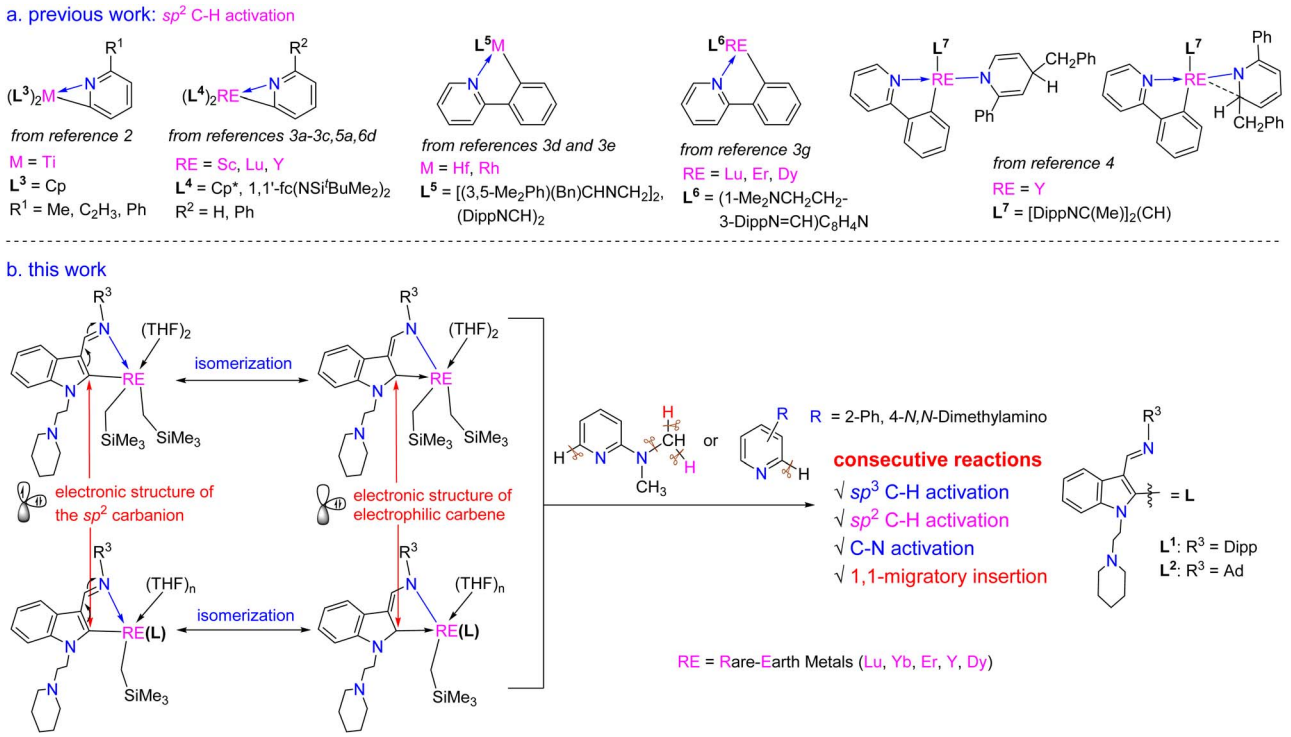

Scheme 1 Reactivity of metal complexes with pyridine derivatives.

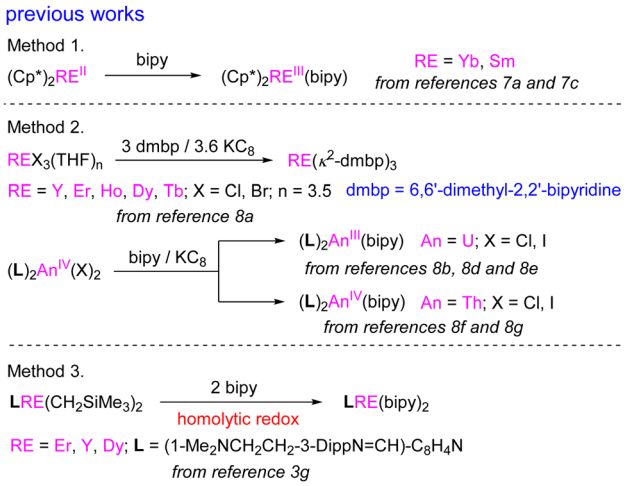

Scheme 2 Prior methods for the preparation of 2,2′-bipyridyl and 6,6′-dimethyl-2,2′-bipyridyl anionic radical complexes.

bipyridyl anionic radical ($bipy^{\bullet-}$) complex. However, transformation of Sc(III) to Sc(I) is unlikely under such conditions due to the high reducing potential of Sc(III) to Sc(I) and the reactivity of the corresponding bipyridyl anionic radical complex has not been studied. Very recently, Zi and coworkers reported that the reaction of $(Cp^{3tms})_2Th^{IV}I_2$ (Cp^{3tms} = η^5-1,2,4-$(Me_3Si)_3C_5H_2$) with a mixture of bipyridine and KC_8 afforded the thorium 2,2′-bipyridyl metallocene $(Cp^{3tms})_2Th(bipy)$, in which the bipyridine is a dianionic ligand and the thorium is in the oxidation state of +4. This complex exhibited plenty of reactivities with various molecules to generate one electron or two electron reduction and C–C coupling products.[16] In addition, it has been reported very recently that the reaction of 1,3-bisfunctionalized indol-2-yl rare-earth metal dialkyl complexes with 2,2′-bipyridine produced the bipyridyl anionic radical complexes (Scheme 2, method 3).[3g] However, the reactivity of the corresponding rare-earth metal 2,2′-bipyridyl radical anion complexes has yet been underexplored.

On the other hand, various types of rare-earth metal alkylidene complexes including bridged[17] and mononuclear terminal ones[18] were synthesized since the proposed formation of rare-earth alkylidene complexes by Schumann in 1979.[19] These alkylidene complexes, however, displayed mainly nucleophilic properties. Meanwhile, rare-earth metal complexes with singlet N-heterocarbenes (NHCs)[20] and cyclic (alkyl)(amino) carbenes (CAACs)[21] as supporting ligands have also been reported. However, reactivities like 1,1-migratory insertion and nucleophilic substitution reactions, which are common in traditional late transition metal electrophilic carbenes, are rarely developed except for our recent reports by utilizing the 1,3-bisfunctionalized indol-2-yl ligands (Scheme 3).[22] Also, the synthesis of high-oxidation state rare-earth metal complexes bearing both electrophilic carbene and nucleophilic alkyls faces a great challenge due to their extreme instability and reactivity, which results from the lack of electrons in the d-orbital to form π-backbonding with the rare-earth metal ions to stabilize the corresponding electrophilic carbene.

In view of these points, we designed the chelate ligands bearing a conjugated system (–C=C–C=N), which can produce an sp^2 carbon showing electrophilic character to bond with the

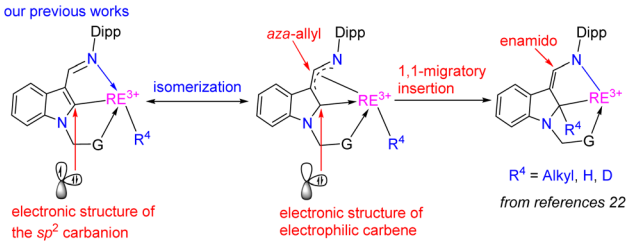

Scheme 3 Rare-earth metal electrophilic carbenes and their 1,1-migratory insertion reactions from our previous studies.

rare-earth metal centre. Thus, a series of 1,3-bisfunctionalized indol-2-yl rare-earth metal complexes bearing electrophilic and nucleophilic carbon centres were synthesized, and their reactivities towards pyridine derivatives were extensively studied with findings of unusual reactivity patterns. Herein, we report these results.

Results and discussion

Synthesis and characterization of the rare-earth metal complexes

The stoichiometric (1 : 1) reactions of the proligand[22c] HL^1 (L^1 = 1-(2-*N*-$C_5H_{10}NCH_2CH_2$)-3-(2,6-$^iPr_2C_6H_3N$=CH)-C_8H_5N) (see the ESI†) with $RE(CH_2SiMe_3)_3\cdot(THF)_2$ (RE = Lu, Yb, Er, Y, Dy) at room temperature afforded the corresponding rare-earth metal dialkyl complexes (κ^2-L^1)$RE(CH_2SiMe_3)_2\cdot(THF)_2$ [RE = Lu(**1a**), Yb(**1b**), Er(**1c**), Y(**1d**), Dy(**1e**)] (Scheme 4 and Fig. 1).[22c] In addition, the stoichiometric (2 : 1) reactions of the proligand HL^1 (L^1 = 1-(2-*N*-$C_5H_{10}NCH_2CH_2$)-3-(2,6-$^iPr_2C_6H_3N$=CH)-C_8H_5N) and HL^2 (L^2 = 1-(2-*N*-$C_5H_{10}NCH_2CH_2$)-3-(AdN=CH)-C_8H_5N) (Ad = adamantyl, $C_{10}H_{15}$) (see the ESI†) with $RE(CH_2SiMe_3)_3\cdot(THF)_2$ (RE = Lu, Yb, Er, Y, Dy, Gd) at room temperature afforded the corresponding rare-earth metal monoalkyl complexes (κ^2-L^1)$_2$-$RE(CH_2SiMe_3)\cdot(THF)_n$ [n = 0, RE = Lu(**2a**), Yb(**2b**); n = 1, Er(**2c**), Y(**2d**), Dy(**2e**)] and (κ^2-L^2)$_2RE(CH_2SiMe_3)\cdot THF$ [RE = Yb(**3a**), Er(**3b**), Y(**3c**), Dy(**3d**), Gd(**3e**)] (Scheme 4 and Fig. 1). These complexes are very sensitive to moisture and air. They are soluble in THF and toluene, but slightly soluble in hexane. All complexes were fully characterized by spectroscopic methods, elemental analyses, and single crystal X-ray diffraction studies. The diamagnetic complexes **1a**, **1d**, **2a**, **2d** and **3c** were further characterized by the NMR spectroscopic method (see the ESI†). The methylene protons of the –CH_2SiMe$_3$ moiety in **3c** exhibited a signal at −0.11 ppm. The methylene protons of the Y–CH_2-SiMe$_3$ (**1d**) gave doublet resonances at −0.20 ppm due to coupling with the yttrium ion ($^2J_{Y-H}$ = 5.0 Hz), which is comparable with the results reported in the literature (−0.43 ppm for the methylene protons of the Y–CH_2SiMe$_3$, $^2J_{Y-H}$ = 3.0 Hz in {[η^1–μ–η^1-3-(CyNCH(CH_2SiMe$_3$))Ind]Y(THF)$_2$(CH_2-SiMe$_3$)}$_2$).[23] The signals centred at 40.8, 50.7 and 55.1 ppm in the

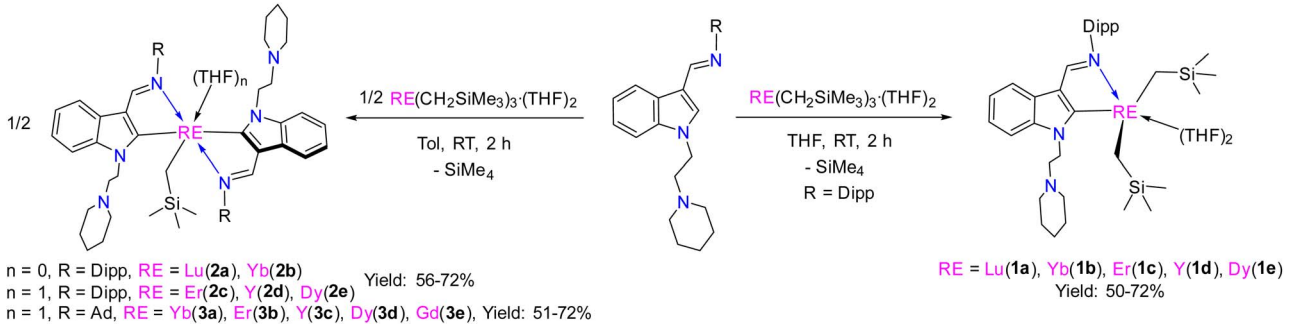

Scheme 4 Synthesis of the rare-earth metal complexes **1–3**.

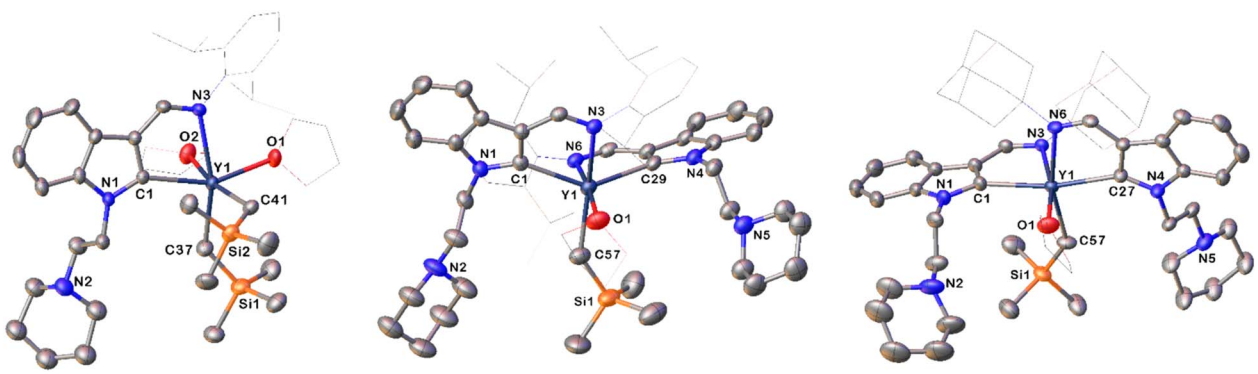

Fig. 1 Representative molecular structures of **1d** (left), **2d** (middle) and **3c** (right) with the thermal ellipsoid at 30% probability level. All hydrogen atoms are omitted and the diisopropylphenyl (Dipp) group, the adamantyl (Ad) group and the carbon atoms of THF are drawn in wireframe style for clarity.

$^{13}C\{^1H\}$ spectra for **1d**, **2d** and **3c** were assigned to the methylene carbons of the Y–CH_2SiMe_3 coupled to the yttrium nucleus with $^1J_{Y-C}$ = 36.3 Hz, 37.5 Hz, and 37.5 Hz, respectively. In addition, the signals centred at 204.1, 205.8, and 205.2 ppm for the corresponding **1d**, **2d** and **3c** in the $^{13}C\{^1H\}$ spectrum were assigned to the indol-2-yl carbon ($C_{2\text{-ind}}$) coupled to the yttrium nucleus with $^1J_{Y-C}$ = 43.8 Hz, 50.0 Hz, and 50.0 Hz, respectively, which correlate with previous results (202.0 ppm for the indol-2-yl carbon ($C_{2\text{-ind}}$)) with $^1J_{Y-C}$ = 50.0 Hz,[22b] but are shifted downfield in comparison with the resonance at 197.1 ppm as observed in the NHC carbene carbon $^1J_{Y-C}$ = 25.0 Hz in $L^{Mes}YCH_2TMS(THF)$ (L^{Mes} = 1-(3-(2,6-^{i}Pr$_2$C$_6$H$_3$N=CH)C$_8$H$_4$N)-CH_2CH_2-3-(2-CH_2-4,6-Me$_2$C$_6$H$_2$)-(N(CH)$_2$NC)).[22b] The ^{89}Y NMR spectra of **1d** and **3c** have resonances at δ = 1101.5 and 773.0 ppm, respectively, which are within the wide range of reported organometallic yttrium complexes[30] (Fig. S14 and S22 in the ESI†). The 1,3-bisfunctionalized indol-2-yl ligands are all bonded to the rare-earth metal ion in the κ^2 form, which is different from the κ^3 bonding mode found in the dimeric chloride complexes,[24] probably due to the coordination of THF and steric effects.

Reactivity of the rare-earth metal complexes with pyridine derivatives

Given the importance of pyridine derivatives as molecular platforms in drug design and the motive to acquire meaningful insights in understanding catalytic reaction mechanisms, we performed stoichiometric reactions of the above-synthesized complexes with pyridine derivatives.

Reactions of the rare-earth metal complexes with 2-*N*,*N*-dimethylaminopyridine. Unique consecutive sp^3 C–H activation/1,1-migratory insertion/C–N activation through intramolecular redox. The stoichiometric (1 : 1) reactions of the dialkyl complexes **1** with 2-*N*,*N*-dimethylaminopyridine in toluene at room temperature afforded the complexes $L^{1\text{-}a}RE(\eta^2$-*N*,*N*-2-MeNPy)(THF) [RE = Lu(**4a**), Yb(**4b**), Er(**4c**), Y(**4d**)] ($L^{1\text{-}a}$ = 1-(2-*N*-C$_5$H$_{10}$NCH$_2$CH$_2$)-3-(2,6-^{i}Pr$_2$C$_6$H$_3$NCH)-2-(methinyl)-C$_8$H$_4$N) in good yields (Scheme 5 and Fig. 2). The ^{89}Y NMR spectrum of **4d** shows a resonance at δ = 880.7 ppm, which is in the range of reported yttrium complexes[30] (see Fig. S29 in the ESI†). Single crystal X-ray structural analyses reveal that these complexes are composed of an unusual 1,3-bisfunctionalized indol-2-methinyl ligand, and 2-*N*-methylamidopyridine. The latter possibly originated from 2-*N*,*N*-dimethylaminopyridine through consecutive sp^3 C–H activation and C–N bond cleavage. The unexpected 1,3-bisfunctionalized indol-2-methinyl ligand is proposed to result from a unique sequence of sp^3 C–H activation of 2-*N*,*N*-dimethylaminopyridine/1,1-migratory insertion/C–N bond cleavage through intramolecular redox, C–H activation and dimerization (see Scheme S5 in the ESI†). To the best of our knowledge, this reactivity pattern is unprecedented in the reactions of transition metal complexes with pyridine derivatives.

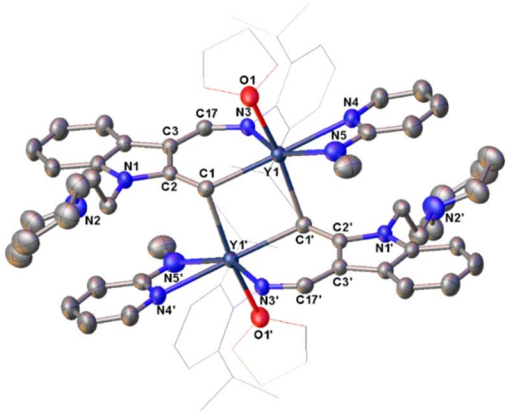

Fig. 2 Representative molecular structure of **4d**. All hydrogen atoms are omitted and the diisopropylphenyl (Dipp) group and the carbon atoms of THF are drawn in wireframe style for clarity.

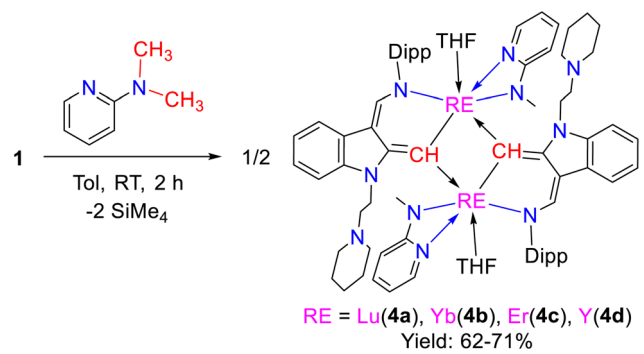

Scheme 5 Reactions of **1** with 2-*N*,*N*-dimethylaminopyridine.

The reaction process of **1d** with 2-*N*,*N*-dimethylaminopyridine is then investigated by DFT calculations, which is in agreement with experimental results. The calculations reveal that the C1 (indol-2-yl carbon) of the indolyl shows electrophilic character with a natural charge of −0.19823 owing to the lack of electrons in the p-orbital, while the Y–C65 and Y–C80 bonds of the Y–CH_2SiMe_3 are strongly polarized with the natural charges of −1.66362 and −1.64763 for the C65 and C80 (see the ESI†), respectively, exhibiting strong nucleophilic properties. First, the dissociation of two THF molecules provides the vacant site for the coordination of the pyridine amine in **B**, in which the C1 (indol-2-yl carbon) of the indolyl displays even higher electrophilicity (natural charge −0.15301). This indicates that the coordination of the strongly electron-donating ligand with the central metal facilitates the formation of the rare-earth metal electrophilic carbene. The formation of intermediate **B** is computed to be endothermic by 6.7 kcal mol^{-1}. Second, the C–H activation of the methyl group of the pyridine amine in **TS(B–C)** results in the formation of tetramethyl silane. Intrinsic coordinate calculation for this transition state yields methylene (pyridine amine) connection to the yttrium (**C**) and dissociation of silane, which is favoured by 21.5 kcal mol^{-1}. The release of silane and re-coordination of the THF molecule to the metal centre in the next step leads to the formation of a stable intermediate (**D**), in which the C1 (indol-2-yl carbon) is more electrophilic than the one in **1d** (natural charge: −0.15925 in **D** *vs.* −0.19823 in **1d**), and is exothermic by 12.2 kcal mol^{-1}. In the

next step, the barrier for the 1,1-migratory insertion of the methylene group of the pyridine amine to the electrophilic carbon C1 [**TS(D–E)**] is favoured over the 1,1-migratory insertion of the CH_2SiMe_3 group to the C1 [**TS(D–E′)**] by 5.9 kcal mol^{-1}. This suggests that the coordination of a donor THF not only promotes the formation of the electrophilic carbene, but also stabilizes the intermediate thereby promoting the selective 1,1-migratory insertion. The consecutive transition state [**TS(E–F)**] *via* the Y–C1 (indol-2-yl carbon) bond cleavage leads to the C–N bond breakage (intramolecular redox) giving a stable intermediate (**F**), exothermic by 44.2 kcal mol^{-1}. Electron rearrangement from **F** to **G** followed by C–H activation of the methylene group [**TS(G–H)**, barrier = 24.3 kcal mol^{-1}] leads to the formation of tetramethyl silane and **H**. The latter isomerizes and dimerizes to form the final product, **4d** (Scheme 6 and see more details in the ESI†).

The above proposed and computed mechanism involved the formation of the intermediate **G**, which bears a methylene group being connected to the indol-2-yl carbon. Therefore, we have carried out a VT-NMR test to track the reaction of complex **1a** with 2-*N*,*N*-dimethylaminopyridine from 263 K to 293 K (Fig. S25 in the ESI†). The formation and disappearance of intermediate **G** can be clearly observed from the spectra as indicated by the appearance and disappearance of H^b of the CH_2SiMe_3 (see Fig. S25 in the ESI†), which provides support for the results of DFT calculations and the proposed mechanism. Unfortunately, our attempts to isolate the intermediate **G** from the reaction of **1** with 2-*N*,*N*-dimethylaminopyridine were unsuccessful. However, the stoichiometric (1 : 1) reactions of the complexes **2** with 2-*N*,*N*-dimethylaminopyridine in toluene at room temperature afforded a mixture of $(\mathbf{L^{1\text{-}b}})_2RE(\eta^2\text{-}N,N\text{-}2\text{-MeNPy})$ [RE = Lu(**5a**), Yb(**5b**), Er(**5c**), Y(**5d**)] ($\mathbf{L^{1\text{-}b}}$ = 1-(2-*N*-$C_5H_{10}NCH_2CH_2$)-3-(2,6-$^{i}Pr_2C_6H_3N{=}CH$)indol-2-methylenyl) (Fig. 3) and $(\mathbf{L^1})_2RE(\eta^2\text{-}N,N\text{-}2\text{-MeNPy})$ [RE = Lu(**6a**), Yb(**6b**), Er(**6c**), Y(**6d**)]. Complexes **6** can also be directly obtained through the reaction of complexes **2** with 2-methylaminopyridine with improved yields (Scheme 7), which is similar to the results reported recently.[3g] X-ray analyses reveal that complexes **5** contain a novel functionalized indol-2-methylenyl ligand, which provides indirect support for the proposed intermediate **G** in the formation of **4**. The formation of the complexes **5** may involve a sequence as follows: the interaction of the

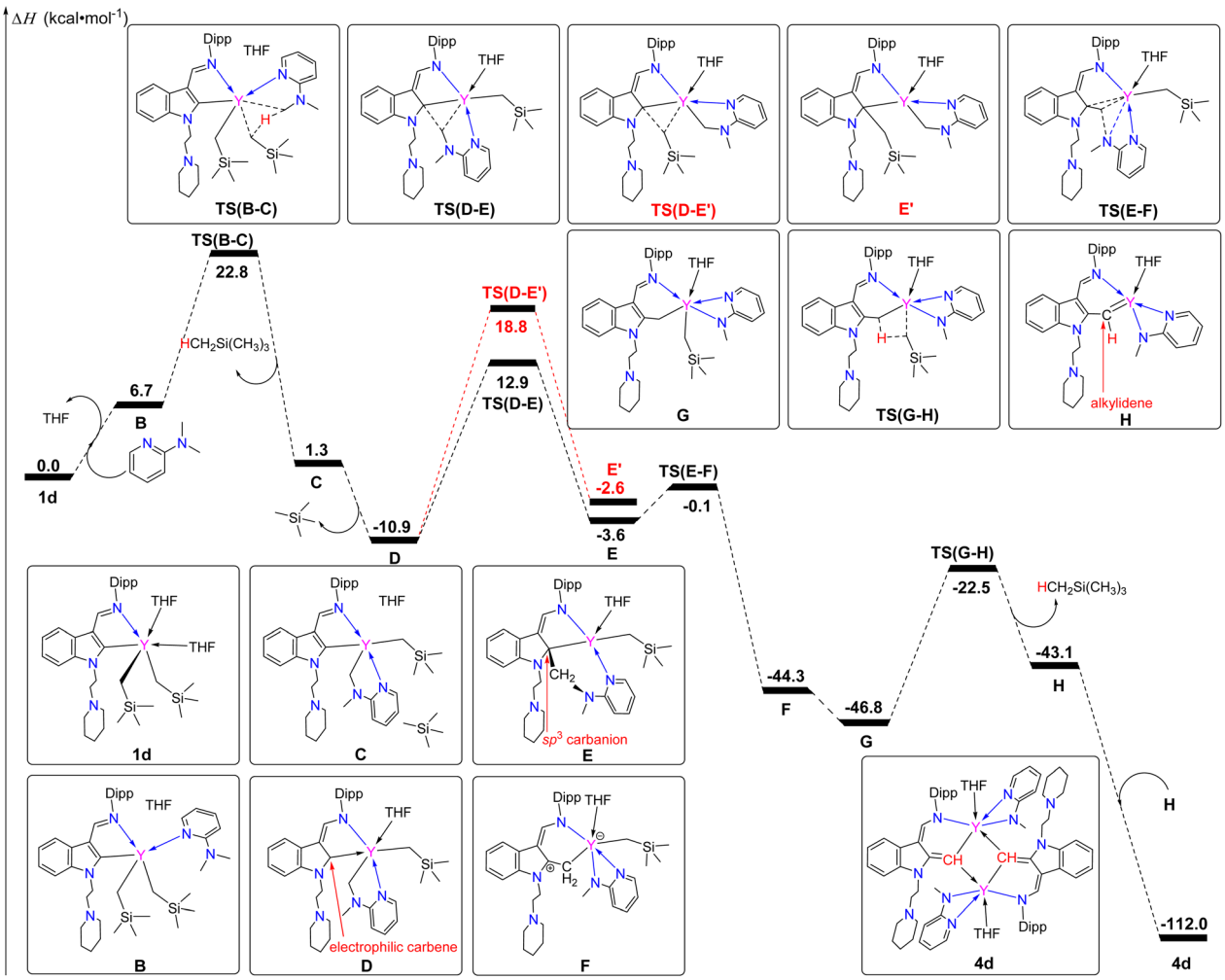

Scheme 6 Computed enthalpy profile for the formation of **4d** from **1d** at room temperature. The enthalpy is given in kcal mol^{-1}.

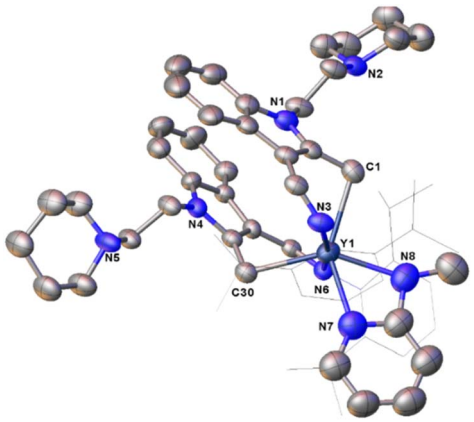

Fig. 3 Representative molecular structure of **5d**. All hydrogen atoms are omitted and the diisopropylphenyl (Dipp) group is drawn in wire-frame style for clarity.

nucleophilic alkyl CH_2SiMe_3 with the sp^3 C–H bond of the 2-*N*,*N*-dimethylaminopyridine through σ-bond metathesis gives the intermediate **A2**, which then undergoes 1,1-migratory insertion to produce the intermediate **A4** possibly driven by the electrophilic character of the indol-2-yl carbon (see the ESI†). Then the breakage of the Y–C bond leads to the cleavage of the C–N bond (intramolecular redox), followed by electron rearrangement to afford the intermediate **A5**, which then interacts with another molecule of **A5** to deliver the final ligand redistribution complexes **5** and **6** (Scheme 8).

The formation of complexes **5d** and **6d** from **2d** has also been investigated computationally (see Scheme S6 in the ESI†). The reaction mechanism is quite similar to that presented in Scheme 6, except that in the last step the lack of a second silyl ligand stops the following C–H activation and dimerization and favours the formation of complexes **5d** and **6d** (−57.8 kcal mol^{-1}) (see the ESI†). Notably, the indol-2-yl carbon of **2d** still exhibits some electrophilic character (natural charge of −0.25) as compared to the highly nucleophilic alkyl carbon (natural charge of −1.69). This charge difference might explain why the first step is the proton transfer from 2-*N*,*N*-dimethylaminopyridine to the alkyl with a kinetically accessible barrier of 23.4 kcal mol^{-1}. After releasing the silane from the coordination sphere, a C–C bond is formed *via* 1,1-migratory insertion between the nucleophilic carbon of *ortho*-metallated 2-*N*,*N*-dimethylaminopyridine and the electrophilic carbon of the indol-2-yl ligand in **A3** (natural charge of −0.21) with an accessible barrier of 29.6 kcal mol^{-1}.

When complexes **3**, which bear an adamantyl group on the imino nitrogen, were reacted with 2-*N*,*N*-dimethylaminopyridine in a 1 : 1 ratio in toluene at room temperature, different complexes $\mathbf{L^2L^{2\text{-}a}}$RE(THF) [RE = Er(**7a**), Y(**7b**)] ($\mathbf{L^{2\text{-}a}}$ = 1-(2-*N*-$C_5H_{10}NCH_2CH_2$)-3-(AdNCH)-2-(3-$Me_2NC_5H_3N$)-C_8H_4N) (Ad = adamantyl, $C_{10}H_{15}$) were isolated in moderate yields (Scheme 7 and Fig. 4). Comparison of the structures between **5** and **7** highlights the influence of the electronic and steric effects of the ligands on the reactions. The formation of **7** involves the activation of the sp^2 C–H bond of the *ortho* pyridine ring by the nucleophilic alkyl CH_2SiMe_3 *via* σ-bond metathesis, forming a three-membered ring intermediate **B1**, which then undergoes a 1,1-migratory insertion reaction to the electrophilic carbon of the indol-2-yl carbon to form the intermediate **B2**. Finally, coordination of the 2-dimethylamino group to the metal centre cleaves the Y–C (indol-2-yl carbon) bond accompanied by an intramolecular redox reaction resulting in the reduction of the pyridine ring, and the final complexes **7** bearing the dearomatic pyridine and indolyl rings are obtained (Scheme 9). From the structural parameters of **7b** (Fig. 4), it can be seen that the imino group of one of the ligands transforms into an amido group with a bond length of Y–N(3) 2.250(3) Å, which can be compared

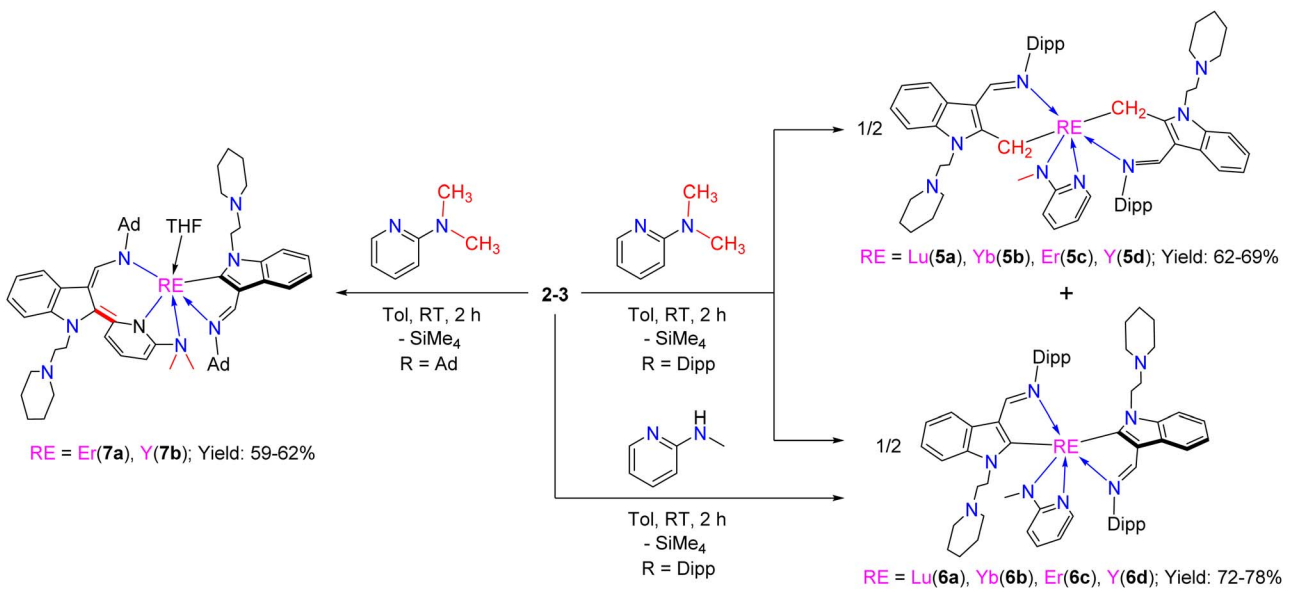

Scheme 7 Reactions of **2–3** with 2-*N*,*N*-dimethylaminopyridine and 2-*N*-methylaminopyridine.

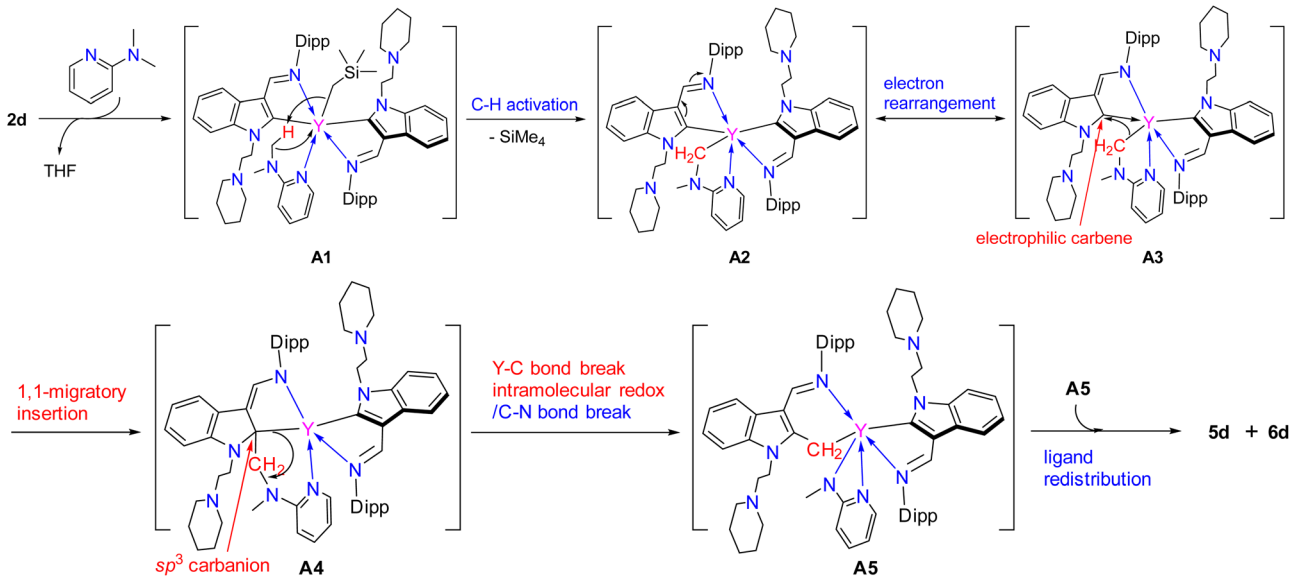

Scheme 8 Possible mechanism for the reaction between **2d** and 2-*N*,*N*-dimethylaminopyridine.

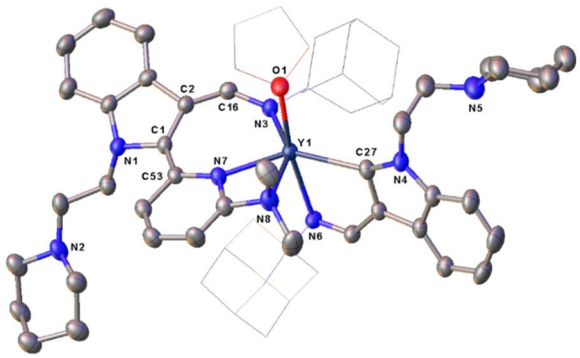

Fig. 4 Representative molecular structure of **7b**. All hydrogen atoms are omitted and the adamantyl (Ad) group is drawn in wireframe style for clarity.

with the Y–N single bond distance (2.254(4) Å) in the complex $[\kappa^3$-(*N*,*N*,*N*)-2-$(Me_2NCH_2CH_2N{=}CH)C_8H_5N]Y[N(SiMe_3)_2]$[25] with the same coordination number. In addition, the indol-2-yl carbon of the ligand bonds with the *ortho*-carbon of pyridine ring with a bond length of C(1)–C(53) 1.362(5) Å, suggesting a double bond character. Thus, dearomatization of the pyridine ring forms a negative nitrogen bonding to the metal with a bond length of Y–N(7) 2.296(3) Å, which is quite shorter than that of 2.376(5) Å found in **5**, in which the bond between the rare-earth metal centre and pyridine nitrogen is a coordination bond (Scheme 7 and Fig. 4).

Besides, our efforts to effect the reactions of 2-*N*,*N*-dimethylaminopyridine with the rare-earth metal monoalkyl complexes bearing 1-methyl (or benzyl)-3-(2,6-^{i}Pr$_2$C$_6$H$_3$N=CH) indolyl ligands resulted only in unidentified mixtures, indicating that the piperidyl moiety attached to the 1-indolyl motif might render the indol-2-yl carbon more electrophilic.

Reactions of the complexes with 2-phenylpyridine. Tandem sp^2 C–H activation, 1,1-migratory insertion and proton abstraction reactions. Encouraged by the above findings, we then studied the stoichiometric (1 : 1) reactions of the complexes **2** with 2-phenylpyridine in toluene at room temperature. To our surprise, two different kinds of complexes, namely, $(\mathbf{L^1})_2$RE(η^2-*N*,*C*-2-phenylpyridyl) [RE = Er(**8a**), Y(**8b**)], and $\mathbf{L^1L^{1\text{-}c}}$Dy(THF) (**9**) ($\mathbf{L^{1\text{-}c}}$ = 1-(2-*N*-$C_5H_{10}NCH_2CH_2$)-3-(2,6-^{i}Pr$_2$C$_6$H$_3$NCH)-2-(2-phenyl-C_5H_3N)-C_8H_5N) were isolated in moderate yields (Scheme 10). The formation of complexes **8**

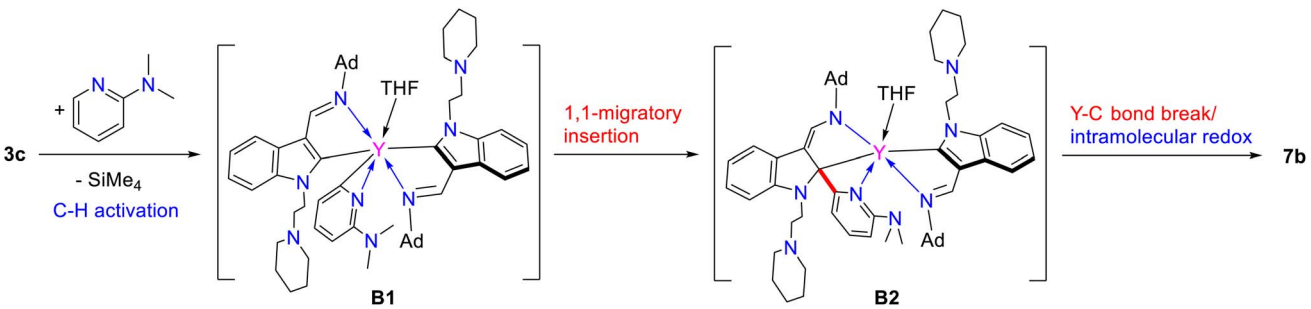

Scheme 9 Possible mechanism for the reaction between **3c** and 2-*N*,*N*-dimethylaminopyridine.

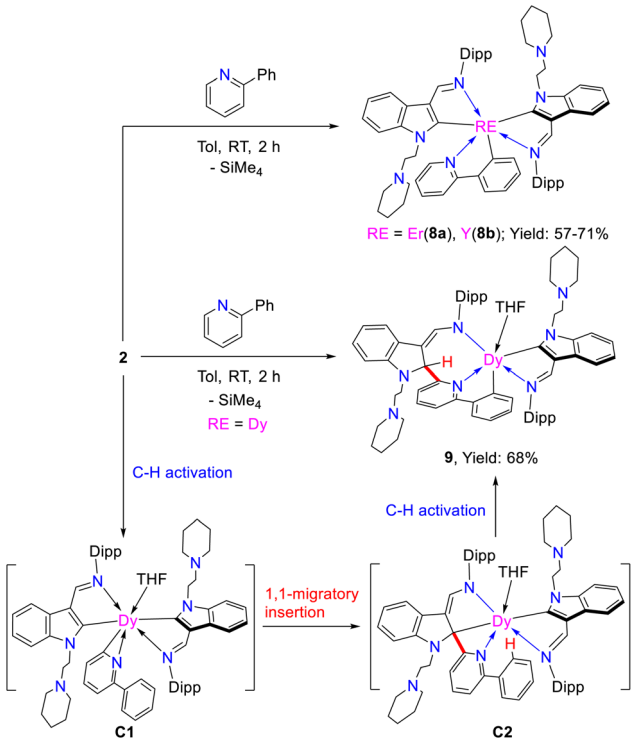

Scheme 10 Reaction of **2** with 2-phenylpyridine.

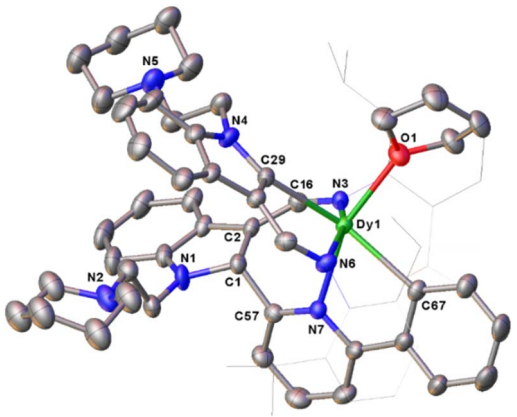

Fig. 5 The molecular structure of **9**. All hydrogen atoms are omitted and the diisopropylphenyl (Dipp) group is drawn in wireframe style for clarity.

involves only the activation of the sp^2 C–H bond, and this reactivity pattern is similar to that in previous reports.[3g,5c–e,g] In addition, the signal centred at 192.0 ppm for the complex **8b** in the $^{13}C\{^1H\}$ spectrum was assigned to the phenyl carbon coupled to the yttrium nucleus with $^1J_{Y-C} = 37.5$ Hz. This is obviously located upfield as compared to those (203.2 to 205.8 ppm) of the indol-2-yl carbon observed in **1d**, **2d**, and **3c**, which may be attributed to the electrophilic character of the indol-2-yl carbon. But the resonance at 192.0 ppm for the carbanion in **8b** is comparable with the result reported in the literature (190.8 ppm for the phenyl carbon and $^1J_{Y-C} = 41.6$ Hz in $\{N^2O\}Y(\eta^2\text{-}N,C\text{-}2'\text{-phenylpyridyl})_2(THF)$, ($\{N^2O\}^-$ = bis(imino)phenoxy)).[5e] Compared to **1d** and **3c**, the resonance of the ^{89}Y NMR of **8b** (501.0 ppm, Fig. S43 in the ESI†) shifted high field possibly due to the coordination of 2-phenylpyridine.[30] However, when the rare-earth metal is dysprosium(III), which has a larger ionic radius than Er^{3+} and Y^{3+}, the corresponding monoalkyl complex reacted with 2-phenylpyridine in toluene at room temperature to produce complex **9**. This differs from not only the formation of **8** but also the result reported recently,[3g] and might be attributed to the electronic and steric effects of the supporting ligand. Specifically, we propose that the interaction of the *ortho* sp^2 C–H bond of the 2-phenylpyridine ring with the nucleophilic alkyl CH_2SiMe_3 through σ-bond metathesis forms a three-membered ring **C1**, which is similar to that in the formation of **7** and previously reported reaction process of rare-earth metal alkyls or hydrides with pyridine derivatives.[3a–d,5b] Then, a 1,1-migratory insertion to the electrophilic carbon of the indol-2-yl gives the tertiary carbon bonded to the metal centre **C2**, which then activates the sp^2 C–H bond of the phenyl ring to afford the final complex **9** (Scheme 10). To our knowledge, this reactivity pattern is also unprecedented in the reactions of transition metal complexes with 2-phenylpyridine. From the structural parameters of **9** (Fig. 5), it is found that the indolyl system was dearomatized and the imino nitrogen was transformed to amido with a Dy–N(3) bond length of 2.333(4) Å, which can be compared with the Dy–N distance of 2.250(3) Å found in the literature.[22b] Such a process is also different from that leading to **7**, which involves an intramolecular redox reaction leading to dearomatization of the pyridine ring.

Reactions of the complexes with 4-*N*,*N*-dimethylaminopyridine (DMAP). Tandem sp^2 C–H activation and 1,1-migratory insertion reactions. In the mechanism proposed above, there are some important intermediates such as **E**, **A4**, **B2**, and **C2** (Scheme 12), all of which bear a tertiary indol-2-yl carbon bonding (RE–$C_{tertiary}$ bond) with the central metal ion. Cleavage of the RE–$C_{tertiary}$ bond plays a crucial role in the formation of **4**, **5** and **7** *via* intramolecular redox, and in the formation of **9** *via* σ-bond metathesis. In order to isolate these key intermediates bearing the RE–$C_{tertiary}$ bond to get more insights into the above reaction processes, we next studied the reactivity of rare-earth metal complexes bearing both electrophilic and nucleophilic carbon centres with other pyridine derivatives like 4-*N*,*N*-dimethylaminopyridine (DMAP), which is less sterically demanding than 2-*N*,*N*-dimethylaminopyridine and has only one coordination site to the central metal ions. When complexes **2** and **3** were treated with 2 equiv. of DMAP in toluene at room temperature, the complexes $\mathbf{L^1L^{1\text{-}d}}$RE(DMAP) [RE = Er(**10a**), Y(**10b**), Dy(**10c**)] ($\mathbf{L^{1\text{-}d}}$ = 1-(2-*N*-$C_5H_{10}NCH_2CH_2$)-3-(2,6-^{i}Pr$_2$C$_6$H$_3$NCH)-2-(4-*N*,*N*-$Me_2NC_5H_3N$)-C_8H_4N) and $\mathbf{L^2L^{2\text{-}b}}$Dy(DMAP) (**11**, $\mathbf{L^{2\text{-}b}}$ = 1-(2-*N*-$C_5H_{10}NCH_2CH_2$)-3-(AdNCH)-2-(4-*N*,*N*-$Me_2NC_5H_3N$)-C_8H_4N) (Ad = adamantyl, $C_{10}H_{15}$) were isolated in moderate yields (Scheme 11). All of these complexes were fully characterized by spectroscopic methods, elemental analyses and single crystal X-ray analyses. From the crystal structures of these complexes (Fig. 6), it can be seen that the complexes **10** and **11** feature a tertiary indol-2-yl carbon connected to the metal centre with a Y–C bond length of 2.565(6) Å. C(30)–C(44)–N(6) [C(30)–C(44) (1.386(8) Å), C(44)–N(6) (1.392(7)

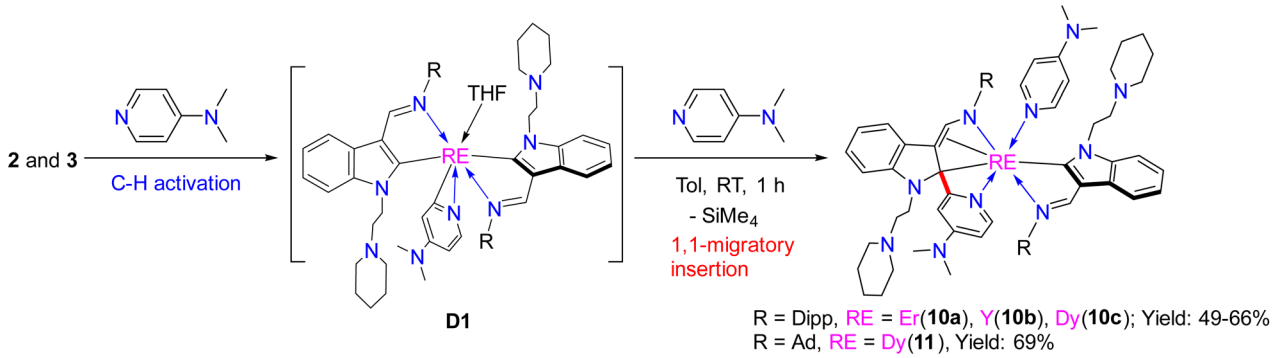

Scheme 11 Reaction of 2 and 3 with DMAP.

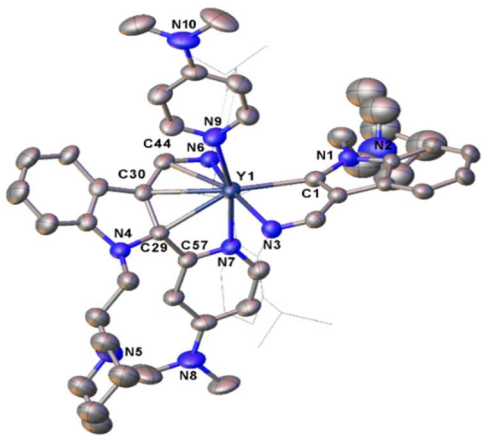

Fig. 6 Representative molecular structure of 10b. All hydrogen atoms are omitted and the diisopropylphenyl (Dipp) group is drawn in wire-frame style for clarity.

Å)] forms an aza-allyl (or amido-ene) conjugated system bonded with the central metal with the Y(1)–C(30) distance of 2.656(6) Å, Y(1)–C(44) distance of 2.597(6) Å, and Y(1)–N(6) distance of 2.229(5) Å, which can be compared with the Y–N bond length (2.242(5) Å) in the literature.[22b] In addition, the C(29)–C(30) and C(29)–C(57) distances are 1.491(8) Å and 1.468(8) Å, respectively, which can be compared with the C–C single bond distance. The formation of the ligand systems ($L^{1\text{-}d}$ or $L^{2\text{-}b}$) in **10** and **11** is proposed to involve the interaction of the nucleophilic alkyl CH_2SiMe_3 with the *ortho* sp^2 C–H of the pyridine ring through σ-bond metathesis to form a three-membered ring metallacycle **D1**. This metallacycle would then undergo 1,1-migratory insertion to the indol-2-yl carbon to produce the final $L^{1\text{-}d}$ or $L^{2\text{-}b}$ (Scheme 11) after ligand exchange of DMAP with THF. The driving force for the migration might be partly due to electrophilic character of the indol-2-yl carbon as revealed by DFT calculations of complex **2d**. This reactivity pattern is different from the cross-carbanion coupling reaction of the *ortho* substituted pyridine derivatives at a rare-earth metal centre.[26] These results also contrast those in previously reported reactions of rare-earth metal alkyls or hydrides with pyridine derivatives, where only the three-membered ring metallacycles[3a–d,5b] or the pyridine coupled products[6] were isolated. While the 1,1-(2-pyridyl) migratory insertion is parallel to the 1,1-alkyl migratory insertion reported previously,[22a] this reaction involves an aryl sp^2 carbon migratory insertion. These results thus provide strong evidence for the existence of **E**, **A4**, **B2**, and **C2** (Scheme 12) as key intermediates in the formation of complexes **4**, **5**, **7**, and **9**, as well as the ensuing proposed mechanistic ways leading to these complexes.

Thus, three different reactivity patterns of the *ortho*-pyridine C–H bond with the synthesized rare-earth metal alkyls were found in this work. (1) The *ortho* pyridine C–H bond activation and 1,1-migratory insertion followed by the intramolecular redox provided complexes **7** when complexes **3** bearing an adamantyl functionalized ligand were treated with 2-*N*,*N*-dimethylaminopyridine. (2) The *ortho* pyridine C–H bond activation and 1,1-migratory insertion followed by abstraction of H produced complex **9** when complex **2e** was reacted with 2-phenylpyridine. (3) The *ortho* pyridine C–H bond activation accompanied by 1,1-migratory insertion delivered complexes **10** and **11** when complexes **2** and **3** were reacted with 4-*N*,*N*-dimethylaminopyridine, indicating that steric, electronic and

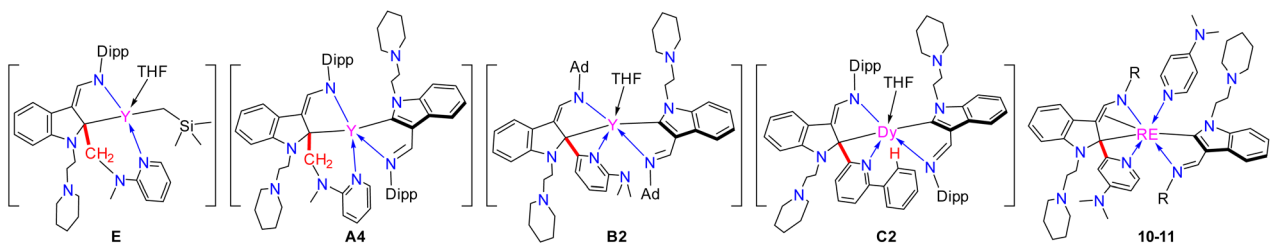

Scheme 12 Structure comparison between important intermediates E, A4, B2, C2 and complexes 10–11.

coordination effects of substrates, substituents of the ligands, and ionic radii of the central metal have significant influence on the reactivity patterns. The isolation and characterization of some complexes structurally similar to the proposed key intermediates provide important evidence in understanding the reaction processes.

Reactions of the rare-earth metal monoalkyl complexes with 2,2′-bipyridine. The bipyridyl anionic radical complexes produced by a homolytic redox reaction and their redox properties. As pointed out above, the reported methods for the generation of the bipyridyl anionic radical complexes utilized the reactions of low-valent metal complexes with 2,2′-bipyridine[7] or treatment of a mixture of metal complexes and 2,2′-bipyridine in the presence of an alkaline metal or KC_8.[8] We have reported the coordination-promoted homolytic reactions of the RE–X (RE = rare-earth metal, X = N, C) bonds to produce the divalent rare-earth metal complexes[27] and homolytic cerium(IV) alkyl and aryl complexes can also provide cerium(III) products.[29] Therefore, we proposed a conceptual idea that the reaction of an external, unsaturated and strong donor ligand such as 2,2′-bipyridine with rare-earth metal alkyls, where the RE^{3+}/RE^{2+} has high reductive potential, would promote the homolytic cleavage of the RE–alkyl bonds while reducing the unsaturated 2,2′-bipyridine (Scheme 13). In line with this hypothesis, our recent studies on the reactions of rare-earth metal dialkyl complexes with 2,2′-bipyridine indeed delivered the bipyridyl anionic radical complexes.[3g] However, the reactivity of monoalkyl rare-earth metal complexes with 2,2′-bipyridine and reactivity of the resulting bipyridyl radical rare-earth metal complexes have not been investigated. Then, we tried the stoichiometric (1 : 1) reactions of the complexes **2** and **3** with 2,2′-bipyridine in toluene at room temperature, the corresponding reactions indeed afforded complexes $(\mathbf{L^1})_2$RE(bipy$^{\bullet-}$) [RE = Yb(**12a**), Er(**12b**), Y(**12c**), Dy(**12d**)] and $(\mathbf{L^2})_2$Er(bipy$^{\bullet-}$) (**13**) with bipyridyl anionic radical ligation in moderate yields (Scheme 14 and Fig. 7). The GC-MS analysis of the reaction mixtures after hydrolysis shows an *m*/*z* peak at 174.25, which might be attributed to the alkyl Me_3SiCH_2 radical coupling product of $[(Me_3SiCH_2)_2]^+$ (see the ESI†). Therefore, the reaction provides a synthetic method for the generation of the bipyridyl radical anions. Compared with the sterically induced reduction (SIR) method proposed by Evans's group,[31] both methods release free radicals and reduce unsaturated substrates. In the present case, complexes **2** are inert to the addition of a weak coordination substrate like chlorobenzene to the toluene solution (see Fig. S50 in ESI†), while the homolytic redox reaction simultaneously happens upon the addition of 2,2′-bipyridine. This implies that the coordination capacity of the substrate may play a key role in the reaction while steric effects cannot be ruled out. From the crystal structural parameters of complexes **12–13**, it can be seen that the bond lengths of the $C_{bipy}-C'_{bipy}$ are 1.414(5) Å, 1.413(8) Å, 1.412(6) Å, 1.407(9) Å and 1.41(2) Å, respectively, which are consistent with the reported bond length of bipy$^{\bullet-}$ (1.43 Å) in the literature,[3g,13,28] but deviate from those of bipy^0 and bipy^{2-} (1.49 Å and 1.38 Å).[8f,11,13,28] The generation of

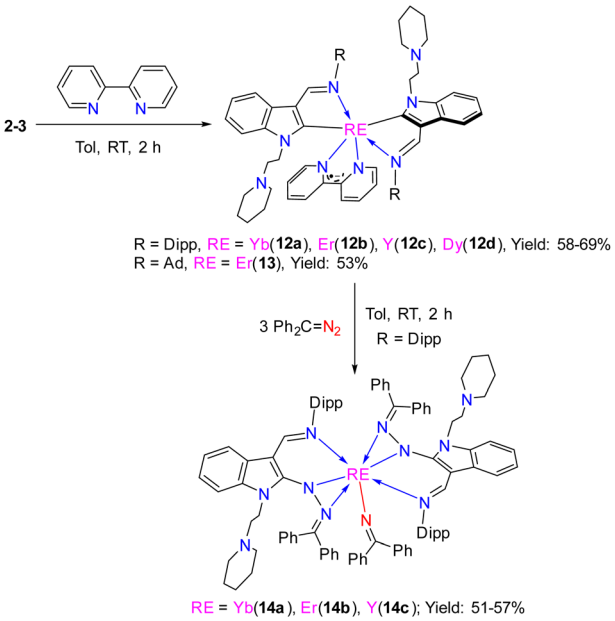

Scheme 14 Reactions of **2–3** with 2,2′-bipyridine and reactions of the bipyridyl complexes with diphenyldiazomethane.

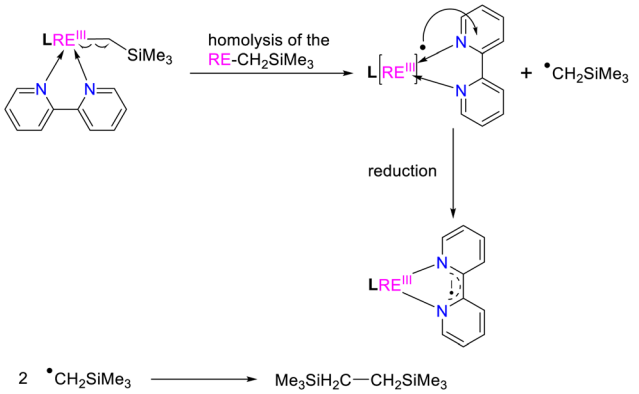

Scheme 13 Proposed homolytic redox reaction (HRR) for the generation of the bipyridyl radical anion.

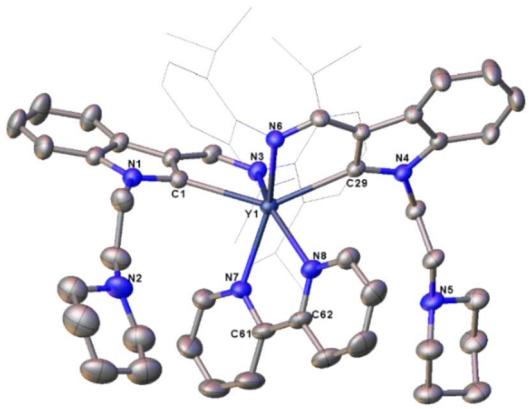

Fig. 7 Representative molecular structure of **12c**. All hydrogen atoms are omitted and the diisopropylphenyl (Dipp) group is drawn in wire-frame style for clarity.

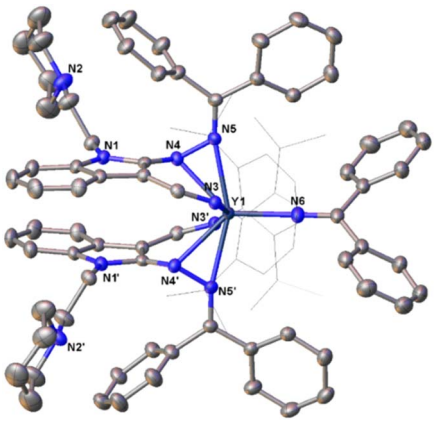

Fig. 8 Representative molecular structure of **14c**. All hydrogen atoms are omitted and the diisopropylphenyl (Dipp) group is drawn in wire-frame style for clarity.

the bipyridyl anionic radical was further proved by EPR analysis (see Fig. S98 in the ESI†) with a resonance at $g = 2.004$, which is similar to that of $(NN^{fc})Y(bipy^{Ph})$ (NN^{fc} = 1,1′-fc(NSi^tBuMe_2)$_2$) (g = 2.0048) produced from the reaction of a corresponding yttrium alkyl complex with 2 equiv. of 2-phenylpyridine.[6d] The UV/vis spectra of complexes **12–13** in THF solution have been studied (see Fig. S99 in the ESI†). The strong absorption band at 200–400 nm can be attributed to the transition of the aromatic ring's π–π* or the charge transfer of the ligand to the metal center. The absorption band at 500 nm and several weak broad absorption bands in the range of 700–1000 nm are due to the characteristic absorption band of the bipyridyl radical anion, which are consistent with the reported results.[3g,7a,8a,14]

Although the bipyridyl anionic radical rare-earth metal complexes can be obtained with different methods, the reactivity of the corresponding bipyridyl anionic radical rare-earth metal complexes is rarely developed. Then, the reactivity of the bipyridyl anionic radical ligated complexes were explored. The stoichiometric (1 : 3) reactions of the rare-earth metal bipyridyl anionic radical ligated complexes **12** with diphenyldiazomethane afforded the redox complexes bearing an iminato group ($\mathbf{L^{1\text{-}e}}$)$_2$RE(N=CPh$_2$) [RE = Yb(**14a**), Er(**14b**), Y(**14c**)] ($\mathbf{L^{1\text{-}e}}$ = 1-(2-*N*-$C_5H_{10}NCH_2CH_2$)-3-(2,6-^{i}Pr$_2$C$_6$H$_3$N=CH)-2-(Ph$_2$C=N$_2$)-C$_8$H$_4$N) (Scheme 14 and Fig. 8). Similar to the formation of **7**, the reactions of diphenyldiazomethane with the indol-2-yl carbon may follow a sequence of coordination, 1,1-migratory insertion and RE–$C_{2\text{-ind}}$ bond cleavage with an intramolecular redox process. This indicates that the bipyridyl ligated complexes show redox properties to reduce the N=N double bond of the diphenyldiazomethane to produce the iminato ligated complexes **14**, which is parallel to the reported reactions of the bipyridyl actinide complexes with unsaturated small molecules.[8b,d-g] However, the reactivity of the bipyridyl anionic radical rare-earth metal complexes with unsaturated substrates is rare.

Conclusions

In summary, a series of rare-earth metal complexes bearing both electrophilic and nucleophilic moieties were synthesized by applying the conjugated system (–C=C–C=N) with an sp^2 carbon being bonded to the metal centres. DFT calculations and experimental results reveal that the indol-2-yl carbon displays electrophilic character that can undergo a 1,1-migratory insertion reaction as the late transition metal electrophilic carbenes did, while the carbon of alkyls bonded to the metal centre exhibits nucleophilic properties to activate sp^3 and sp^2 C–H bonds of the pyridine derivatives *via* σ-bond metathesis. Studies on the reactions of the synthesized complexes with pyridine derivatives lead to disclosure of different reactivity patterns including: (1) unprecedented consecutive C–H activation/1,1-migratory insertion/C–N and C–H activation delivering the 1,3-bisfunctionalized indol-2-methinyl rare-earth metal complexes when the dialkyl complexes were treated with 2-*N*,*N*-dimethylaminopyridine; (2) the consecutive C–H activation/1,1-migratory insertion/C–N bond activation producing the indol-2-methylenyl rare-earth metal complexes when the monoalkyl complexes were reacted with 2-*N*,*N*-dimethylaminopyridine; (3) the tandem C–H activation/1,1-migratory insertion affording the 2-(2-[4-*N*,*N*-dimethylamino]pyridyl)-indol-2-yl rare-earth metal complexes when the monoalkyl complexes were reacted with 4-*N*,*N*-dimethylaminopyridine, and (4) homolytic redox reaction (HRR) generating the 2,2′-bipyridyl anionic radical complexes when the monoalkyl complexes were treated with 2,2′-bipyridine. These reactions provide helpful insights in understanding and designing relevant catalytic reactions. It is also found that the coordination of the strongly electron-donating ligand with the central metal facilitates the formation of the rare-earth metal electrophilic carbene. Isolation and characterization of some intermediate equivalents provide important evidence for understanding these multiple-step reaction processes. The findings in this work provide useful methods to access different dearomatic indolyl or functionalized indolyl complexes. Furthermore, the reactions of the rare-earth metal monoalkyl complexes with 2,2′-bipyridine provided a conceptually new route to bipyridyl anionic radical ligated complexes, which show redox properties towards diphenyldiazomethane delivering the iminato group by reduction of the N=N double bond of the diphenyldiazomethane. To the best of our knowledge, the reactivity patterns found in this paper are completely distinct from those of transition metal alkyls or hydrides with pyridine derivatives previously reported, highlighting the uniqueness of the rare-earth metal complexes bearing both electrophilic and nucleophilic carbon centres.

Data availability

Experimental procedures, X-ray crystallographic details, NMR and infrared spectroscopy data, and computational details are available in the ESI.† CCDC 2278697–2278701, 2348805–2348814 and 2348816–2348844 contain the supplementary crystallographic data for this paper.

Author contributions

W. Wu led and performed the synthesis, reactivity study of the complexes, characterization experiments of complexes, and

manuscript draft writing. T. Rajeshkumar performed the DFT calculations under the supervision of L. Maron. D. Hong and Z. Huang assisted in the X-ray data collection and refinement. F. Chai, S. Zhu and Q. Yuan assisted in the analysis of experimental data. L. Maron participated in the discussion on DFT calculation results. S. Wang was responsible for the project design, discussion, manuscript writing, and editing.

Conflicts of interest

There are no conflicts to declare.

Acknowledgements

We are grateful for the financial support from the National Natural Science Foundation of China (No. 22031001 and U23A2079) and the grants from the Anhui Province (202305a12020018, GXXT-2021-052).

References

1 (*a*) J. A. Bull, J. J. Mousseau, G. Pelletier and A. B. Charette, *Chem. Rev.*, 2012, **112**, 2462–2713; (*b*) C. Allais, J. Grassot, J. Rodriguez and T. Constantieux, *Chem. Rev.*, 2014, **114**, 10829–10868; (*c*) M. Escolano, D. Gaviña, G. Alzuet-Piña, S. Díaz-Oltra, M. Sánchez-Roselló and C. Del Pozo, *Chem. Rev.*, 2024, **124**, 1122–1246; (*d*) Y. Nakao, K. S. Kanyiva and T. Hiyama, *J. Am. Chem. Soc.*, 2008, **130**, 2448–2449; (*e*) Y. Nakao, Y. Yamada, N. Kashihara and T. Hiyama, *J. Am. Chem. Soc.*, 2010, **132**, 13666–13668; (*f*) Q. Chen, X. M. D. Jourdin and P. Knochel, *J. Am. Chem. Soc.*, 2013, **135**, 4958–4961; (*g*) G. Wang, J. Cao, L. Gao, W. Chen, W. Huang, X. Cheng and S. Li, *J. Am. Chem. Soc.*, 2017, **139**, 3904–3910; (*h*) Q. Sun, P. Chen, Y. Wang, Y. Luo, D. Yuan and Y. Yao, *Inorg. Chem.*, 2018, **57**, 11788–11800; (*i*) A. Kundu, M. Inoue, H. Nagae, H. Tsurugi and K. Mashima, *J. Am. Chem. Soc.*, 2018, **140**, 7332–7342; (*j*) C. Han, Y. Liu, X. Tian, F. Rominger and A. S. K. Hashmi, *Org. Lett.*, 2021, **23**, 9480–9484; (*k*) J. Liu, Y. Li, J. Jiang, Y. Liu and Z. Ke, *ACS Catal.*, 2021, **11**, 6186–6192; (*l*) J.-B. Ma, X. Zhao, D. Zhang and S.-L. Shi, *J. Am. Chem. Soc.*, 2022, **144**, 13643–13651; (*m*) H. Cao, D. Bhattacharya, Q. Cheng and A. Studer, *J. Am. Chem. Soc.*, 2023, **145**, 15581–15588.

2 E. Klei and J. H. Teuben, *J. Organomet. Chem.*, 1981, **214**, 53–64.

3 (*a*) L. Waston, *J. Chem. Soc., Chem. Commun.*, 1983, **6**, 276–277; (*b*) M. E. Thompson, S. M. Baxter, A. R. Bulls, B. J. Burger, M. C. Nolan, B. D. Santarsiero, W. P. Schaefer and J. E. Bercaw, *J. Am. Chem. Soc.*, 1987, **109**, 203–219; (*c*) K. H. D. Haan, Y. Wielstra and J. H. Teuben, *Organometallics*, 1987, **6**, 2053–2060; (*d*) H. Tsurugi, K. Yamamoto and K. Mashima, *J. Am. Chem. Soc.*, 2011, **133**, 732–735; (*e*) H. Kaneko, H. Nagae, H. Tsurugi and K. Mashima, *J. Am. Chem. Soc.*, 2011, **133**, 19626–19629; (*f*) L. Qu, T. Roisnel, M. Cordier, D. Yuan, Y. Yao, B. Zhao and E. Kirillov, *Inorg. Chem.*, 2020, **59**, 16976–16987; (*g*) S. Zhu, W. Wu, D. Hong, F. Chai, Z. Huang, X. Zhu, S. Zhou and S. Wang, *Inorg. Chem.*, 2024, **63**, 14860–14875.

4 Y. Zhang, J. Zhang, J. Hong, F. Zhang, L. Weng and X. Zhou, *Organometallics*, 2014, **33**, 7052–7058.

5 (*a*) B. J. Deelman, W. M. Stevels, J. H. Teuben, M. T. Lakin and A. L. Spek, *Organometallics*, 1994, **13**, 3881–3891; (*b*) E. Lu, J. Chu, Y. Chen, M. V. Borzov and G. Li, *Chem. Commun.*, 2011, **47**, 743–745; (*c*) B.-T. Guan and Z. Hou, *J. Am. Chem. Soc.*, 2011, **133**, 18086–18089; (*d*) G. Luo, Y. Luo, J. Qu and Z. Hou, *Organometallics*, 2012, **31**, 3930–3937; (*e*) G. Song, W. N. O. Wylie and Z. Hou, *J. Am. Chem. Soc.*, 2014, **136**, 12209–12212; (*f*) G. Song, B. Wang, M. Nishiura and Z. Hou, *Chem.–Eur. J.*, 2015, **21**, 8394–8398; (*g*) R. Azpíroz, A. Di Giuseppe, A. Urriolabeitia, V. Passarelli, V. Polo, J. J. Perez-Torrente, L. A. Oro and R. Castarlenas, *ACS Catal.*, 2019, **9**, 9372–9386.

6 (*a*) C. T. Carver and P. L. Diaconescu, *J. Am. Chem. Soc.*, 2008, **130**, 7558–7559; (*b*) C. T. Carver, D. Benitez, K. L. Miller, B. N. Williams, E. Tkatchouk, W. A. Goddard III and P. L. Diaconescu, *J. Am. Chem. Soc.*, 2009, **131**, 10269–10278; (*c*) C. T. Carver, B. N. Williams, K. R. Ogilby and P. L. Diaconescu, *Organometallics*, 2010, **29**, 835–846; (*d*) B. N. Williams, W. Huang, K. L. Miller and P. L. Diaconescu, *Inorg. Chem.*, 2010, **49**, 11493–11498; (*e*) Y. Shibata, H. Nagae, S. Sumiya, R. Rochat, H. Tsurugi and K. Mashima, *Chem. Sci.*, 2015, **6**, 5394–5399.

7 (*a*) M. Schultz, J. M. Boncella, D. J. Berg, T. Don Tilley and R. A. Andersen, *Organometallics*, 2002, **21**, 460–472; (*b*) C. H. Booth, M. D. Walter, D. Kazhdan, Y.-J. Hu, W. W. Lukens, E. D. Bauer, L. Maron, O. Eisenstein and R. A. Andersen, *J. Am. Chem. Soc.*, 2009, **131**, 6480–6491; (*c*) W. J. Evans and D. K. Drummond, *J. Am. Chem. Soc.*, 1989, **111**, 3329–3335.

8 (*a*) Y. Xiao, R. Sun, J. Liang, Y. Fang, Z. Liu, S. Jiang, B. Wang, S. Gao and W. Huang, *Inorg. Chem. Front.*, 2021, **8**, 2591–2602; (*b*) Y. Heng, T. Li, D. Wang, G. Hou, G. Zi and M. D. Walter, *Organometallics*, 2023, **42**, 91–113; (*c*) S. J. Kraft, P. E. Fanwick and S. C. Bart, *Inorg. Chem.*, 2010, **49**, 1103–1110; (*d*) L. Zhang, C. Zhang, G. Hou, G. Zi and M. D. Walter, *Organometallics*, 2017, **36**, 1179–1187; (*e*) T. Li, D. Wang, Y. Heng, G. Hou, G. Zi and M. D. Walter, *Organometallics*, 2023, **42**, 392–406; (*f*) W. Ren, H. Song, G. Zi and M. D. Walter, *Dalton Trans.*, 2012, **41**, 5965–5973; (*g*) W. Ren, G. Zi and M. D. Walter, *Organometallics*, 2012, **31**, 672–679.

9 T. Mehdoui, J.-C. Berthet, P. Thuery, L. Salmon, E. Riviere and M. Ephritikhine, *Chem.–Eur. J.*, 2015, **11**, 6994–7006.

10 L. Jacquot, M. Xemard, C. Clavaguera and G. Nocton, *Organometallics*, 2014, **33**, 4100–4106.

11 C. R. Stennett, J. Q. Nguyen, J. W. Ziller and W. J. Evans, *Organometallics*, 2023, **42**, 696–707.

12 Y. Lv, C. E. Kefalidis, J. Zhou, L. Maron, X. Leng and Y. Chen, *J. Am. Chem. Soc.*, 2013, **135**, 14784–14796.

13 M. W. Rosenzweig, F. W. Heinemann, L. Maron and K. Meyer, *Inorg. Chem.*, 2017, **56**, 2792–2800.

14 P. L. Diaconescu and C. C. Cummins, *Dalton Trans.*, 2015, **44**, 2676–2683.

15 D. J. Beetstra, A. Meetsma, B. Hessen and J. H. Teuben, *Organometallics*, 2003, **22**, 4372–4374.
16 S. Wang, D. Wang, Y. Heng, T. Li, W. Ding, G. Zi and M. D. Walter, *Inorg. Chem.*, 2024, **63**, 7473–7492.
17 (*a*) H. M. Dietrich, K. W. Törnroos and R. Anwander, *J. Am. Chem. Soc.*, 2006, **128**, 9298–9299; (*b*) W. Ma, C. Yu, Y. Chi, T. Chen, L. Wang, J. Yin, B. Wei, L. Xu, W.-X. Zhang and Z. Xi, *Chem. Sci.*, 2017, **8**, 6852–6856; (*c*) J. Zhou, T. Li, L. Maron, X. Leng and Y. Chen, *Organometallics*, 2015, **34**, 470–476; (*d*) D. S. Levine, T. D. Tilley and R. A. Andersen, *Organometallics*, 2017, **36**, 80–88; (*e*) M. Bonath, C. Maichle-Mössmer, P. Sirsch and R. Anwander, *Angew. Chem., Int. Ed.*, 2019, **58**, 8206–8210; (*f*) J. Hong, L. Zhang, X. Yu, M. Li, Z. Zhang, P. Zheng, M. Nishiura, Z. Hou and X. Zhou, *Chem.–Eur. J.*, 2011, **17**, 2130–2137; (*g*) W.-X. Zhang, Z. Wang, M. Nishiura, Z. Xi and Z. Hou, *J. Am. Chem. Soc.*, 2011, **133**, 5712–5715; (*h*) T. Li, M. Nishiura, J. Cheng, Y. Li and Z. Hou, *Chem.–Eur. J.*, 2012, **18**, 15079–15085; (*i*) V. M. Birkelbach, F. Kracht, H. M. Dietrich, C. Stuhl, C. Maichle-Mössmer and R. Anwander, *Organometallics*, 2020, **39**, 3490–3504; (*j*) C. O. Hollfelder, L. N. Jende, H.-M. Dietrich, K. Eichele, C. Maichle-Mössmer and R. Anwander, *Chem.–Eur. J.*, 2019, **25**, 7298–7302; (*k*) D. A. Buschmann, L. Schumacher and R. Anwander, *Chem. Commun.*, 2022, **58**, 9132–9135; (*l*) J. Scott, H. Fan, B. F. Wicker, A. R. Fout, M.-H. Baik and D. J. Mindiola, *J. Am. Chem. Soc.*, 2008, **130**, 14438–14439; (*m*) R. Litlabø, M. Zimmermann, K. Saliu, J. Takats, K. W. Törnroos and R. Anwander, *Angew. Chem., Int. Ed.*, 2008, **47**, 9560–9564; (*n*) T. E. Rieser, R. Thim-Spöring, D. Schädle, P. Sirsch, R. Litlabø, K. W. Törnroos, C. Maichle-Mössmer and R. Anwander, *J. Am. Chem. Soc.*, 2022, **144**, 4102–4113; (*o*) D. Schadle, R. Litlabø, M. Meermann-Zimmermann, R. Thim-Spöring, C. Schädle, C. Maichle-Mössmer, K. W. Törnroos and R. Anwander, *Inorg. Chem.*, 2024, **63**, 9624–9637.
18 (*a*) W. Mao, L. Xiang, L. Maron, X. Leng and Y. Chen, *J. Am. Chem. Soc.*, 2017, **139**, 17759–17762; (*b*) K. Aparna, M. Ferguson and R. G. Cavell, *J. Am. Chem. Soc.*, 2000, **122**, 726–727; (*c*) D. P. Mills, L. Soutar, W. Lewis, A. J. Blake and S. T. Liddle, *J. Am. Chem. Soc.*, 2010, **132**, 14379–14381; (*d*) M. Fustier, X. F. Le Goff, P. Le Floch and N. Mézailles, *J. Am. Chem. Soc.*, 2010, **132**, 13108–13110; (*e*) W. Mao, L. Xiang, C. A. Lamsfus, L. Maron, X. Leng and Y. Chen, *J. Am. Chem. Soc.*, 2017, **139**, 1081–1084; (*f*) C. Wang, J. Zhou, X. Zhao, L. Maron, X. Leng and Y. Chen, *Chem.–Eur. J.*, 2016, **22**, 1258–1261.
19 H. Schumann and J. Muller, *J. Organomet. Chem.*, 1979, **169**, C1–C4.
20 (*a*) W. Xie, H. Hu and C. Cui, *Angew. Chem., Int. Ed.*, 2012, **51**, 11141–11144; (*b*) M. Zhang, J. Zhang, X. Ni and Z. Shen, *RSC Adv.*, 2015, **5**, 83295–83303; (*c*) K. Lv and D. Cui, *Organometallics*, 2008, **27**, 5438–5440; (*d*) H. Yao, J. Zhang, Y. Zhang, H. Sun and Q. Shen, *Organometallics*, 2010, **29**, 5841–5846; (*e*) W. Fegler, T. P. Spaniol and J. Okuda, *Dalton Trans.*, 2010, **39**, 6774–6779; (*f*) I. V. Lapshin, A. V. Cherkasov, K. A. Lyssenko, G. K. Fukin and A. A. Trifonov, *Inorg. Chem.*, 2022, **61**, 9147–9161; (*g*) Y. Pan, A. Zhao, Y. Li, W. Li, Y.-M. So, X. Yan and G. He, *Dalton Trans.*, 2018, **47**, 13815–13823; (*h*) I. V. Lapshin, A. V. Cherkasov, A. F. Asachenkob and A. A. Trifonov, *Chem. Commun.*, 2020, **56**, 12913–12916; (*i*) Z. Huang, S. Wang, X. Zhu, Q. Yuan, Y. Wei, S. Zhou and X. Mu, *Inorg. Chem.*, 2018, **57**, 15069–15078; (*j*) C. Yao, F. Lin, M. Wang, D. Liu, B. Liu, N. Liu, Z. Wang, S. Long, C. Wu and D. Cui, *Macromolecules*, 2015, **48**, 1999–2005; (*k*) J. Yuan, H. Hu and C. Cui, *Chem.–Eur. J.*, 2016, **22**, 5778–5785; (*l*) Z. Pan, J. Zhang, L. Guo, H. Yang, J. Li and C. Cui, *Inorg. Chem.*, 2021, **60**, 12696–12702.
21 (*a*) Y. Xiao, Z. Liu, J. Liang, K. Yang and W. Huang, *Dalton Trans.*, 2022, **51**, 15873–15882; (*b*) Y. Pan, X. Jiang, Y.-M. So, C. T. To and G. He, *Catalysts*, 2020, **10**, 71–85.
22 (*a*) Z. Huang, R. Wang, T. Sheng, X. Zhong, S. Wang, X. Zhu, Q. Yuan, Y. Wei and S. Zhou, *Inorg. Chem.*, 2021, **60**, 18843–18853; (*b*) D. Hong, T. Rajeshkumar, S. Zhu, Z. Huang, S. Zhou, X. Zhu, L. Maron and S. Wang, *Sci. China: Chem.*, 2023, **66**, 117–126; (*c*) W. Wu, T. Rajeshkumar, D. Hong, S. Zhu, Z. Huang, F. Chai, W. Wang, Q. Yuan, Y. Wei, Z. Xie, L. Maron and S. Wang, *Inorg. Chem.*, 2024, **63**, 18365–18378.
23 G. Zhang, B. Deng, S. Wang, Y. Wei, S. Zhou, X. Zhu, Z. Huang and X. Mu, *Dalton Trans.*, 2016, **45**, 15445–15456.
24 Z. Huang, S. Wang, X. Zhu, Y. Wei, Q. Yuan, S. Zhou, X. Mu and H. Wang, *Chin. J. Chem.*, 2021, **39**, 3360–3368.
25 Y. Wei, J. Gao, L. Jiang, Z. Huang, Q. Bao, Q. Yuan, L. Zhang, S. Zhou and S. Wang, *Organometallics*, 2022, **41**, 2985–2996.
26 W. Liu, Y. Zhao, W. Ma, L. Xu, J. Wei and W.-X. Zhang, *Cell Rep. Phys. Sci.*, 2023, **4**, 101479–101492.
27 (*a*) E. Sheng, S. Wang, G. Yang, S. Zhou, L. Cheng, K. Zhang and Z. Huang, *Organometallics*, 2003, **22**, 684–692; (*b*) K. Zhang, W. Zhang, S. Wang, E. Sheng, G. Yang, M. Xie, S. Zhou, Y. Feng, L. Mao and Z. Huang, *Dalton Trans.*, 2004, **7**, 1029–1037; (*c*) S. Wang, X. Tang, A. Vega, J.-Y. Saillard, S. Zhou, G. Yang, W. Yao and Y. Wei, *Organometallics*, 2007, **26**, 1512–1522; (*d*) S. Zhou, Z. Wu, L. Zhou, S. Wang, L. Zhang, X. Zhu, Y. Wei, J. Zhai and J. Wu, *Inorg. Chem.*, 2013, **52**, 6417–6426.
28 S. Fortier, J. Veleta, A. Pialat, J. Le Roy, K. B. Ghiassi, M. M. Olmstead, A. Metta-Magana, M. Murugesu and D. Villagran, *Chem.–Eur. J.*, 2016, **22**, 1931–1936.
29 B. Feng, L.-W. Ye, N. Wang, H.-S. Hu, J. Li, M. Tamm and Y. Chen, *CCS Chem.*, 2024, DOI: **10.31635/ccschem.024.202404131**.
30 (*a*) C. J. Schaverien, *Organmetallics*, 1994, **13**, 69–82; (*b*) R. E. White and T. P. Hanusa, *Organometallics*, 2006, **25**, 5621–5630; (*c*) L. Latsch, E. Lam and C. Coperet, *Chem. Sci.*, 2020, **11**, 6724–6735.
31 (*a*) W. J. Evans, G. W. Nyce and J. W. Ziller, *Angew. Chem., Int. Ed.*, 2000, **39**, 240–242; (*b*) W. J. Evans, S. A. Kozimor, J. W. Ziller and N. Kaltsoyannis, *J. Am. Chem. Soc.*, 2004, **126**, 14533–14547; (*c*) W. J. Evans, *Inorg. Chem.*, 2007, **46**, 3435–3449.